IEEE Access
Multidisciplinary | Rapid Review | Open Access Journal

Received 19 July 2022, accepted 18 August 2022, date of publication 26 August 2022, date of current version 2 September 2022.

Digital Object Identifier 10.1109/ACCESS.2022.3201896

RESEARCH ARTICLE

Electrically-Small Antenna With Low SAR for Scalp and Deep Tissue Biomedical Devices

SYED MANAF ALI SHAH[1], MUHAMMAD ZADA[2], (Graduate Student Member, IEEE), JAMAL NASIR[1], OWAIS OWAIS[1], AND HYOUNGSUK YOO[2,3], (Senior Member, IEEE)

[1]Department of Electrical and Computer Engineering, COMSATS University Islamabad, Abbottabad Campus, Abbottabad 22060, Pakistan
[2]Department of Electronic Engineering, Hanyang University, Seoul 04763, Republic of Korea
[3]Department of Biomedical Engineering, Hanyang University, Seoul 04763, Republic of Korea

Corresponding author: Hyoungsuk Yoo (hsyoo@hanyang.ac.kr)

This work was supported by the Institute of Information and Communications Technology Planning and Evaluation (IITP) Grant funded by the Korean Government Ministry of Science and ICT (MIST), under Grant 2022-0-00310.

ABSTRACT An ultra-miniaturized implantable antenna for scalp and deep tissue implants operating in the Industrial, Scientific, and Medical (ISM) frequency band is proposed in this communication. The proposed antenna has a compact size of only 4.422 mm^3 ($3.45 \times 3.4 \times 0.377$ mm^3). A meandered patch backed by a full ground plane was used to implement the proposed ultra-miniaturized antenna. The full ground plane does not allow backward energy flow, thus ensuring patient safety. The performance of the proposed antenna was evaluated in three different simulation environments: homogeneous skin phantom (HSP), skin implant multilayer phantom (SIMP), and muscle implant multilayer phantom (MIMP) models with and without a dummy implantable wireless device (IMD). These models were considered to evaluate the performance of the proposed antenna in more realistic complex human body environments. The proposed antenna demonstrated excellent impedance matching performance at the ISM band with a measured -10 dB impedance bandwidth of 260 MHz (2,249–2,511 MHz). The effects of coaxial cable on antenna performance were also studied. The proposed antenna exhibited a maximum measured peak gain of -26.54 dBi. Furthermore, the 1-g and 10-g specific absorption rate (SAR) values were calculated and satisfied the safety guidelines. A reliable communication link up to distances of 15, 4, and 1.3 m for bit rates of 7 kbps, 100 kbps, and 1 Mbps, respectively, can be established between the implantable device and external base station. Finally, a sensitivity analysis of the proposed antenna was conducted showing that the proposed implantable antenna can efficiently work under varying tissue conditions.

INDEX TERMS Communication link, impedance bandwidth, implantable antenna, specific absorption rate, ultra-miniaturized.

I. INTRODUCTION

Implantable wireless devices (IMDs) can measure and collect physiological data from various parts of the patient body such as glucose level, temperature, and heartbeat and transmit the data wirelessly to an external monitoring device [1]. The implantable nature of the IMDs imposes size restrictions on them; thus, there is a need to design miniaturized IMDs without affecting their performance [2]. Designing a miniaturized implantable antenna, a vital component of any IMD, is challenging. Implantable antennas have different radiation characteristics than free space antennas and must be miniaturized, satisfy various patient safety criteria [3], and satisfy various other conditions [4].

The MedRadio band (401–406 MHz) is often used for IMDs, but this band restricts the transmission of high-resolution images due to bandwidth limitations. Moreover, the large wavelength at the 433/686/915 MHz bands makes them unsuitable for the design of miniaturized IMDs due to the bulky device size. Therefore, the Industrial, Scientific, and Medical (ISM) band (2.4 GHz) is the most suitable for designing IMDs with huge transmission data

The associate editor coordinating the review of this manuscript and approving it for publication was Chan Hwang See.

requirements and a small-sized antenna [5]. IMDs operating in this band might not face interference from other services like Bluetooth, Wi-Fi, near-field communication, or IEEE 802.15.4 because these short-range communication systems have ultra-low power transmitters, different modulation schemes, and different effective isotropic radiated power (EIRP) [6].

Much research has been conducted on the design of miniaturized implantable antennas operating at a 2,400 MHz frequency band in recent years. Authors in [7] presented a 2,400 MHz implantable antenna with an ultra-miniaturized size. A small volume of 8 mm^3 was achieved using a chip resistor of 1.2 Ω on the radiating part of the antenna. This configuration resulted in increased losses and fabrication complexities. In [8], a circular-shaped wideband antenna operating in the 2,400 MHz band was presented with a volume of 39.3 mm^3 and a high specific absorption rate (SAR) placing the patient in a hazardous situation.

Similarly, the authors in [9] presented a dual ring slot antenna operating at the 2,450 MHz band for biomedical applications. An array of metamaterial was used over a superstrate to enhance gain, resulting in a bulkier size. Moreover, the presented antenna was not tested inside an IMD; therefore, the effects of IMD circuitry were not studied. In [10], a coplanar waveguide (CPW)-fed patch antenna was proposed to operate at the 2,450 MHz band. The antenna offers high performance but with a bulkier volume of 705 mm^3. Similarly, a four-port multiple-input multiple-output (MIMO) implantable antenna for high data rate applications was presented in [11]. This antenna, consisting of an electromagnetic bandgap (EBG) decoupling structure, has a volume of 434.6 mm^3, which is unsuitable for most IMDs. In [12], a meandered resonator-based dual-port MIMO antenna operating at 2,450 MHz was proposed for medical implant applications with a volume of 3.98 mm^3. Size miniaturization was achieved by meandering the patch and introducing slots in the ground plane. Similarly, in [13] a quad element MIMO antenna operating at a 433 MHz band was proposed for high data rate applications.

The proposed antenna consists of four separate meandered semicircular resonators with a total volume of 23.6 mm^3. A shortening pin was used to achieve size miniaturization. Authors in [14] proposed a dual-band meandered line antenna operating at 910 MHz and 2,450 MHz bands. Size miniaturization was achieved using meandered resonator and a square slot in the ground plane. The proposed antenna had a total volume of 8.41 mm^3. Yausaf *et al.* [15] proposed a multi-band conformal antenna for endoscopic applications. The proposed antenna operates in MedRadio (401–406 MHz), Industrial, Scientific, and Medical (ISM) (433.1–434.8 MHz, 868–868.6 MHz, 902–928 MHz), and midfield (1200 MHz) bands. Acceptable bandwidth and gain performance has been achieved at the desired frequency bands. The antenna, however, has a bulky volume of 57 mm^3 and 48.98 mm^3 in the flat and wrapped form, respectively. Likewise, in [16], an ultra-wideband scalp

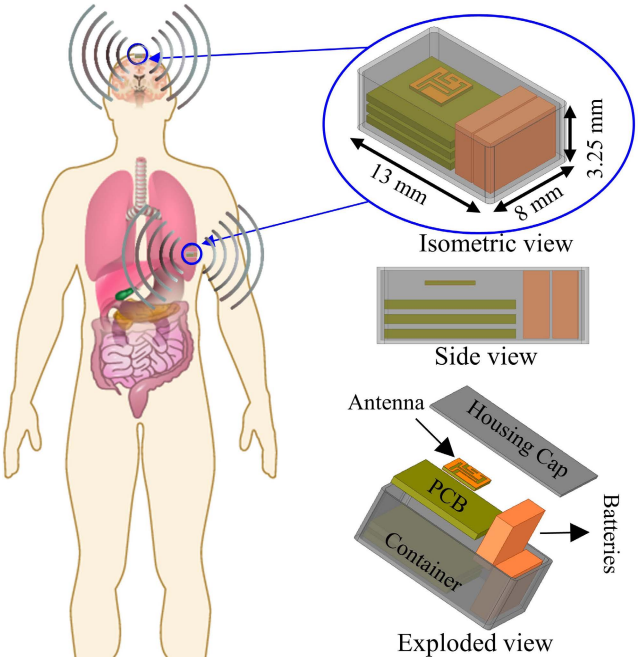

FIGURE 1. Conceptual overview and detailed architecture of scalp/deep implantable device.

implantable antenna operating at ISM (2,400–2,480 MHz) band is proposed. The proposed antenna offers a bandwidth of 1,038.7 MHz and a peak gain of −20.71 dBi with a volume of 9.8 mm^3. The authors in [17] proposed a tri-band ultra miniaturized implantable antenna with a volume of 13.195 mm^3 operating at ISM bands of 902–928 MHz and 2,400–2,483.5 MHz and midfield band of 1,824–1,980 MHz. Acceptable bandwidth and gain performance at the desired frequency bands were obtained. Similarly in [18], the authors reported an ultra-miniaturized antenna for deep implanted biomedical devices operation in the ISM 2,450 MHz band. The proposed antenna had a volume of 7.8 mm^3 and offers a bandwidth and gain of 480 MHz and −16.5 dBi, respectively.

In this communication, we propose an ultra-miniaturized implantable antenna for operation in the 2,450 MHz ISM band. The antenna consists of a meandered patch with a condensed volume of 4.422 mm^3. The proposed antenna outperformed existing implantable antennas in terms of gain, bandwidth, and SAR. Size miniaturization and impedance matching at the desired band of 2,450 MHz is achieved by T-shape, L-shape, and open slots in the radiator only.

Unlike existing implantable antennas, in which miniaturization is achieved either by slots in the ground plane or by using shortening pins or both. In this work no modification is performed in the ground plane and no shorting pin is used for size miniaturization, reducing the back lobe and improving antenna gain performance. A homogeneous skin phantom (HSP) of size 100 × 100 × 100 mm^3 was used for simulation purposes. Moreover, system level study was performed by installing the proposed antenna in a flat-type device that mimics IMD (Figure 1), and the simulations were carried

TABLE 1. Comparison of proposed implantable antenna with previous studies.

Ref.	Antenna size (λg^3)	Frequency (MHz)	SAR 1-g	SAR 10-g	Bandwidth (MHz)	Gain (dBi)	Implantation Depth (mm)	Via /GPM
[10]	(0.125 × 0.125 × 0.0.0061)	2,450	482	31.5	1100	-15	4	N/Y
[16]	0.097×0.097 × 0.0028	2,450	289.7	N/A	1038.7	-20.71	N/A	Y/Y
[18]	0.0904 × 0.0834 × 0.0028	2,450	185.56	N/A	480	-16.5	N/A	Y/Y
[19]	(0.080 × 0.638 ×0.032)	2,400	508	--	310	-22.7	3	Y/Y
[20]	(0.097 × 0.097 × 0.0027)	2,450	350.8	--	1533	-22	12.5	Y/Y
[21]	(0.076 × 0.102 × 0.012)	2,400	270.2	31.4	371	-25.9	-	N/N
[22]	(0.080 × 0.408 × 0.032)	2,400	856.4	92.2	400	-37.3	4	Y/Y
[23]	(0.25 × 0.25 × 0.032)	2,400	486	93.1	540	-33	3	Y/N
This work	**(0.089 × 0.088 × 0.009)**	**2,450**	**141**	**14.2**	**260**	**-26.54**	**10**	**N/N**

GPM: Ground plane modification, Y: Yes, N: No, N/A: Not Available

out in HSP. Afterward, for further validation of the results attained by the device in the HSP, additional simulations were conducted in skin implant multilayer phantom (SIMP) and muscle implant multilayer phantom (MIMP). The maximum gain attained by the proposed antenna inside the skin phantom at 2,450 MHz was −26 dBi.

The SAR of the proposed device was also conducted in the head and deep tissue of the Gostove human model for safety evaluation by using a finite-difference time-domain (FDTD)-based software. Link budget computation for wireless communication and maximum input power calculation were also conducted for the suggested implantable antenna. Sensitivity analysis was also conducted to ensure the acceptable performance of the proposed antenna under varying tissue properties. In addition, the coupling effects of the IMD's components and the proposed antenna were analyzed. The simulated design was fabricated and tested, and the measured results agreed closely with the simulation results. Finally, performance comparison of the proposed antenna with similar implantable antennas recently published was also performed and is presented in Table 1. Based on the comparison of the proposed antenna with similar antennas available (Table 1), the proposed antenna provides adequate performance with an ultra-compact size.

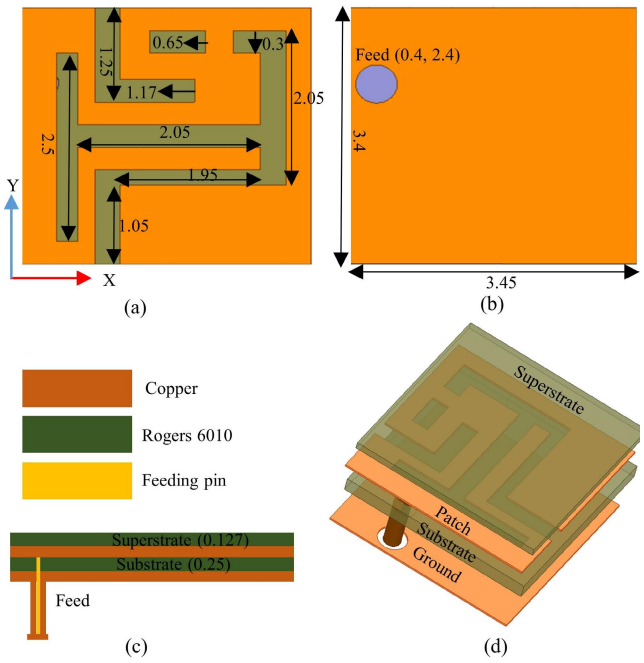

FIGURE 2. Detailed profile proposed antenna (Units: mm): (a) Radiating patch. (b) Ground plane. (c) Side view. (d) Exploded view.

II. METHODOLOGY

A. ANTENNA AND SYSTEM DESIGN

The detailed configuration of the proposed ultra-miniaturized implantable antenna is depicted in Figure 2. Rogers RT/duroid® 6010 laminates ($\varepsilon_r = 10.2$, $\tan\delta = 0.0035$) with thicknesses of 0.25 and 0.127 mm are used as the substrate and superstrate, respectively. The high permittivity substrate shortens the effective wavelength and decreases antenna losses, contributing to size miniaturization. The use of the superstrate serves two purposes; size miniaturization and decoupling the antenna from the lossy surrounding environment [3], [24]. Roger materials are not biocompatible; therefore, the proposed antenna is covered with a thin layer of ceramic alumina (Al_2O_3) with a permittivity of 9.8 to achieve biocompatibility.

The radiator is created with meandered lines of variable lengths to produce a highly miniaturized antenna and obtain resonance at 2,450 MHz. These meandered lines on the

radiating patch increase the current path, which reduces the size considerably. Furthermore, a full ground plane backs the radiator, resulting in no backward energy leakage. This results in reduced backward radiation resulting in low back lobe, subsequently improving the gain and safety of the patient.

In the proposed design, miniaturization in size is attained by the slots in the radiating patch; the overall volume of the antenna is only $3.45 \times 3.4 \times 0.377$ mm^3 (4.422 mm^3). For measurements, a semi-flexible 50 Ω coaxial cable is used to connect the antenna to a vector network analyzer (VNA). For optimal impedance matching, the excitation is given at a location of X = 0.4 mm and Y = 2.4 mm. For skin and muscle tissue implants, the antenna is integrated with a flat type IMD with a volume of $13 \times 8 \times 3.25$ mm^3, as depicted in Figure 1. The proposed IMD consists of batteries, electronic components, sensors, and the proposed implantable antenna. Rogers RT/duroid® 6010 is used for the sensors and electronic components, while a perfect electric conductor (PEC) is used for the battery packs [2]. For biocompatibility of the IMD, the proposed antenna with all the components is encapsulated in biocompatible ceramic alumina (Al_2O_3) with a permittivity of 9.8 and thickness of 0.25 mm. In the HSP environment, an implantation depth of 5 mm is considered. For a SIMP environment, the implantation depth remains the same. However, below the skin, fat and muscle layers are added. Similarly, for MIMP, the IMD is placed in muscle at a depth of 10 mm. Figure 3 illustrates these setups.

B. SIMULATION AND MEASUREMENT ENVIRONMENTS

The proposed ultra-miniaturized implantable antenna (with and without a system) was modeled and designed using a finite element method (FEM)-based simulator (HFSS). Initially, the simulations were conducted in an HSP of dimensions $100 \times 100 \times 100$ mm^3 with a depth of 5 mm and enclosed by a radiation box, as presented in Figure 3(a). The electrical properties of the skin, such as a permittivity (ε_r) of 38 and electrical conductivity (σ) of 1.46 S/m at 2,450 MHz, were considered.

Moreover, SIMP and MIMP composed of skin, fat, and muscle are also constructed to verify the performance of the proposed implantable antenna in a complex human tissue model, as depicted in Figures 3(b) and 3(c). The thickness of the skin, fat, and muscle layers are 20, 20, and 40 mm with an ε_r of 37.88, 5.28, and 54.81 and a σ of 1.44, 0.10, and 2.25, respectively [11], [25]. The difference between heterogeneous (SIMP) and deep tissue (MIMP) models is the depth of the proposed implantable antenna. In the SIMP, the antenna is placed in the skin layer at a depth of 5 mm, while in the MIMP, the antenna is placed in the muscle layer at a depth of 10 mm. The prototype of the proposed antenna was fabricated, and measurements were taken based on the setup depicted in Figures 3(e) and 3(f) to validate the simulated reflection coefficient and radiation pattern. For the measurements, the prototype of the proposed antenna was plunged in minced pork to approximately mimic human tissue properties.

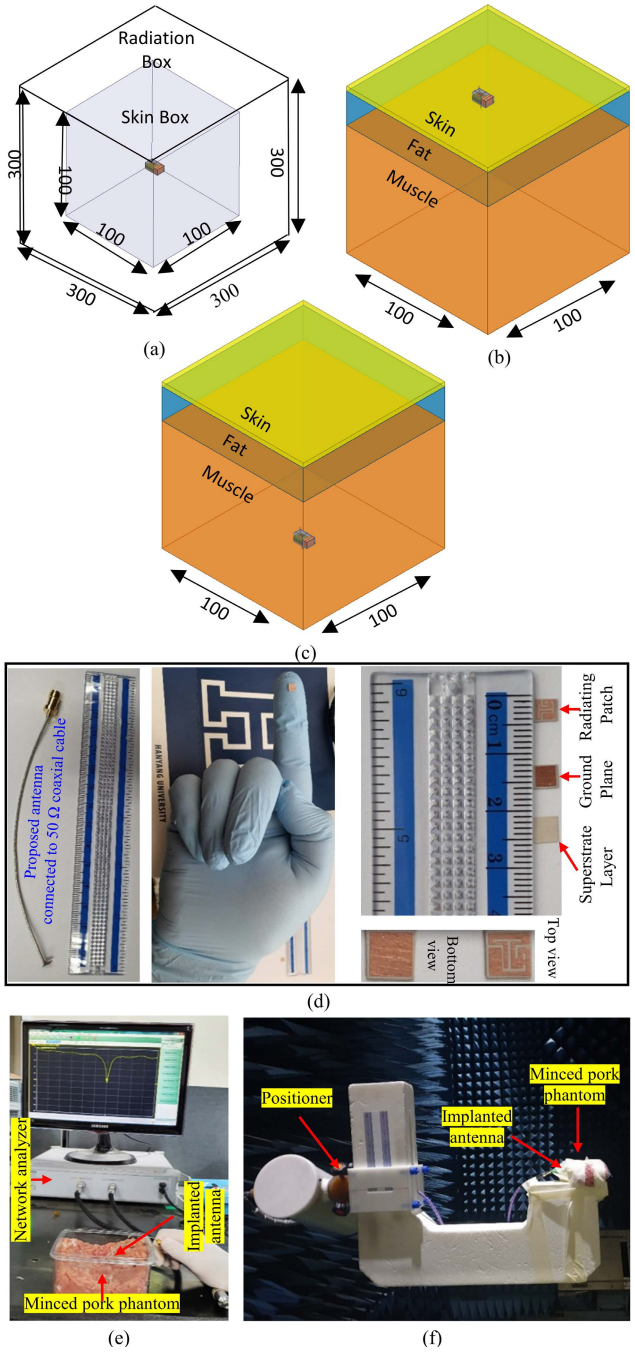

FIGURE 3. Simulation and measurement setups of the proposed multiband implantable antenna (a) HSP model, (b) SIMP model, (c) MIMP model, (d) prototypes of proposed antenna, and (e) measurement setups for reflection coefficient (S_{11}), and (f) radiation pattern.

A three-step process for optimizing the proposed antenna was followed to obtain resonance at the band of interest, as depicted in Figure 4(a). The initial design of the proposed antenna started from a rectangular patch antenna. Then, adding meandered slits in the radiating patch resulted in size miniaturization and impedance matching at the band of interest. The reflection coefficient (S_{11}) and Z-parameters plots of each step are portrayed in Figures 4(b) and 4(c),

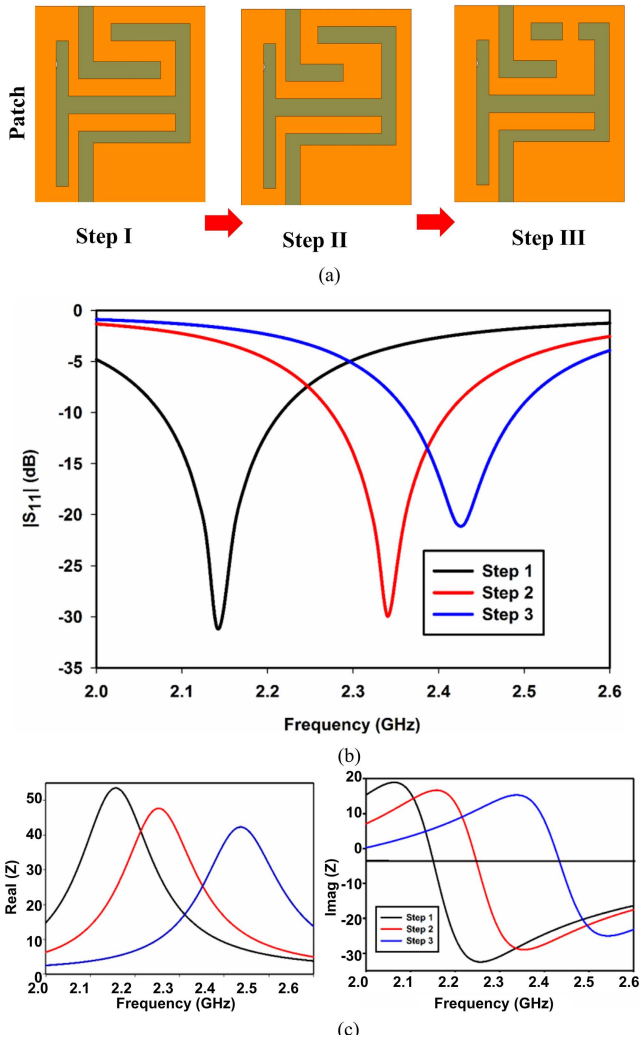

FIGURE 4. (a) Design steps. (b) S_{11} of design steps. (c) Real and imaginary part of impedance for each design step.

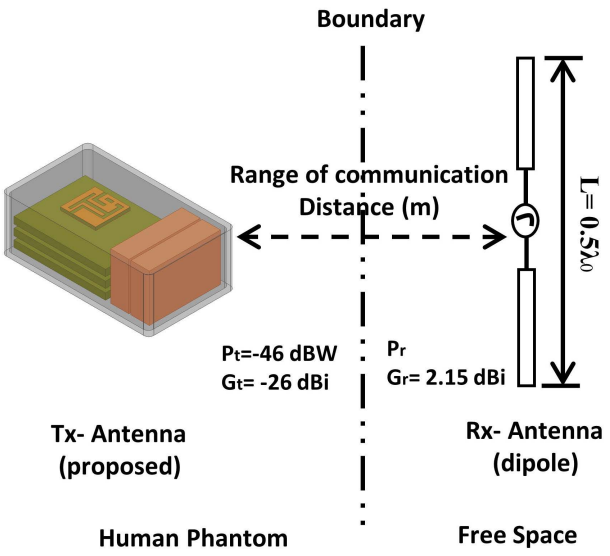

FIGURE 5. Conceptual diagram for the link budget analysis.

TABLE 2. Important parameters used in link budget calculation of proposed antenna.

Parameters	Variable	Value
Frequency (MHz)	f_r	2,450
Antenna Gain (dBi)	G_t	-26
Distance (m)	d	0-15
Transmitter power (dBm)	P_t	-16
Receiver Gain (dBi)	G_r	2.15
Boltzmann Constant	k	1.38×10^{-23}
Path loss (dB)	Lf	distance dependent
Reference distance (m)	d0	1
Path loss exponent	γ	1.5
Shadowing effect (dB)	S	4
Polarization mismatch losses	eP	0.3
Impedance matching of the proposed antenna (dBm)	MLTx	0
Impedance matching of the receiving antenna (dBm)	MLRx	0

respectively. Step I shows that Imag Z is capacitive at the operating frequency while the Re Z is around 7 Ω. In step II, by decreasing the length of the upper L-shaped slot resulted in improving the Re Z to 10 Ω while Imag Z remains capacitive. Finally, in Step III by putting a shortening strip in the top right slot increased the inductance making Imag Z = 0 while Re Z becomes 45 Ω. This resulted in achieving resonance at the desired frequency as clear from Figure 4(b).

C. LINK BUDGET INVESTIGATION FOR WIRELESS COMMUNICATION

The communication link budget is evaluated to analyze the established communication link between the proposed implantable antenna and the external receiving antenna. A schematic setup for the calculation of the link budget is shown in Figure 5. The proposed antenna can be seen as a transmitting antenna, while a dipole antenna acts as a receiving antenna. The standard equations (eq (1) and (2)) in [26], [27], and [28] are used to calculate the link budget by considering losses such as path loss, antenna and material losses, and cable losses. For effective communication, a link margin of 0 dB or greater should be achieved. Therefore, a 20-dB link margin is considered for reliable communication between IMD and the external base station in this study. The critical parameters involved in evaluating the link budget are presented in Table 2.

$$L_m = P_{tx} + G_{tx} + G_{rx} - \frac{E_b}{N_0} + KT_0 + B_r - Loss, \quad (1)$$

here P_{tx}, G_{tx}, and G_{rx} represent the transmitted power (dBm), the gain of the transmitter antenna (dBi), and the gain of the receiving antenna (dBi), $\frac{E_b}{N_0}$ is an ideal phase shift keying, N_0 represents the noise power density (dB/Hz), K is the Boltzmann's constant, T_0 is the temperature in kelvin, and B_r is the data rate in kb/s, respectively. The associated losses

can be described as

$$(Loss)\ dBm = (L_f)\ dBm + (e_p)\ dB + (ML_{tx})\ dBm + (ML_{rx})\ dBm, \quad (2)$$

where L_f, e_P, ML_{tx}, and ML_{rx} represent the path loss, polarization mismatch loss, antenna mismatch loss, and dipole antenna mismatch loss, respectively. For the calculation of path loss, a long-distance model was adapted as follows:

$$(L_f)\ dBm = 10\gamma\ log_{10}(\frac{d}{d_0}) + 20\log_{10}(\frac{4\pi d_0}{\lambda_0}) + (S)\ dB. \quad (3)$$

Here, γ is the path loss environmentally dependent component, d is the distance between the *Tx* and *Rx* antennas, d_0 is the reference distance ($d_0 \leq$ d), λ_0 is the free space wavelength, and *S* is the shadowing effect [28].

D. IMPACT OF IMD COMPONENTS ON THE ANTENNA PERFORMANCE

IMDs contain various components like PCB, RF, and electrical components. The majority of these components are made up of conductive materials, therefore, coupling effect could be produced with the antenna. This coupling affects the impedance matching and radiation performance of the antenna. Therefore, the antenna should be placed at a certain distance from the metallic components inside the IMD to minimize this coupling. In order to find the optimum placement of the antenna in the IMD a parametric analysis was performed, as shown in Figure 6. It can be observed that as the distance 'd' increases matching of the antenna improves. The proposed antenna performed well when it was placed closed to the metallic objects. However, to improve matching at the desired frequency of operation 'd' is chosen as 1 mm. Thus, in the practical scenario styrofoam of 1 mm with a dielectric constant close to 1 should be placed between the antenna and metallic components.

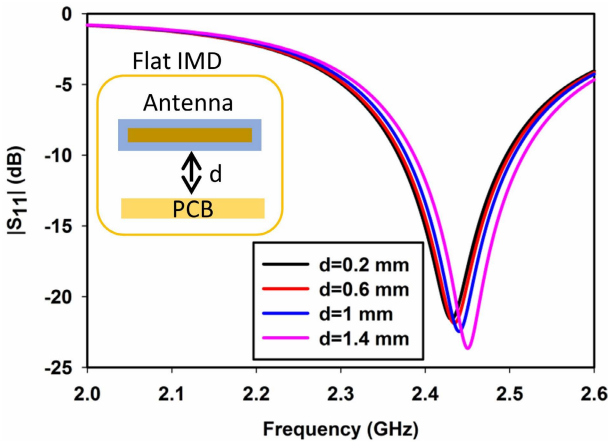

FIGURE 6. Influence on impedance matching of the placement of the metallic objects near the antenna.

III. RESULTS AND DISCUSSION

The proposed miniaturized antenna was fabricated on Rogers RT/duroid® 6010 and placed inside a 3D printed IMD. The prototype of the flat type IMD containing different components along with the proposed antenna is shown in Figure. 7(a) and (b). the sealed device was immersed in minced pork for measuring the return loss through a vector network analyzer (VNA). The simulated and measured return loss of the proposed implantable antenna is presented in Figure 8. The performance of the proposed antenna was evaluated in three different environments, as depicted in Figure 3: HSP, SIMP and MIMP. The return loss of the proposed antenna with and without system integration is also presented in Figure 8. There is a slight shift in resonance frequency after integration with the device.

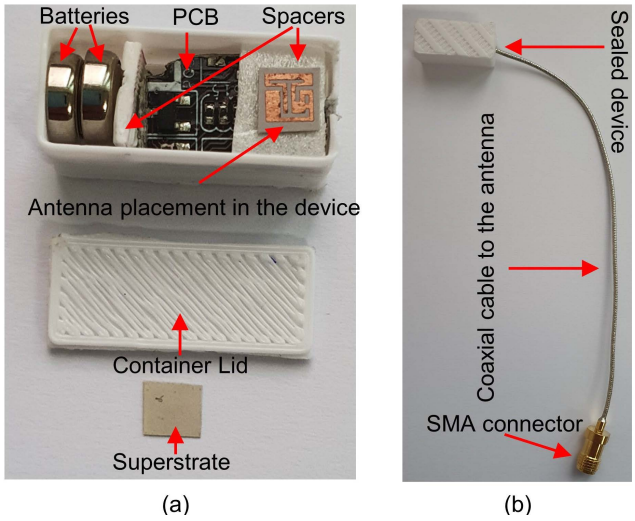

FIGURE 7. 3D printed IMD with dummy electronics. (a) Exploded view of the IMD and (b) sealed IMD with coxial cable for S_{11} measurement.

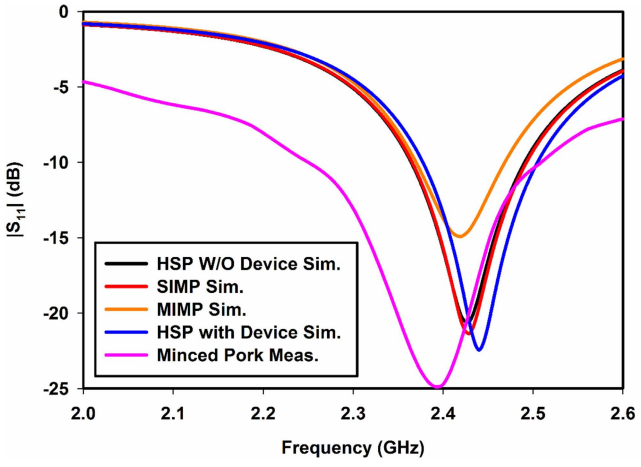

FIGURE 8. Simulated and measured reflection coefficients comparison of the proposed antenna system in different human body tissues with and without device integration.

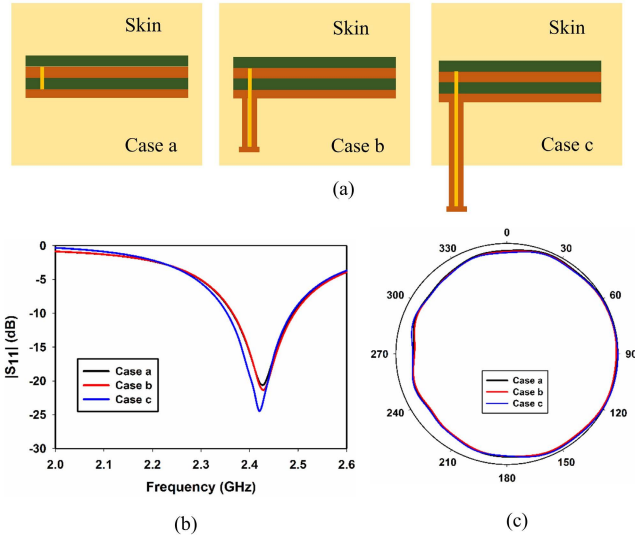

FIGURE 9. Effects of coaxial cable on proposed antenna performance: (a) Different cases for coaxial cable. (b) Reflection coefficient comparison. (c) Radiation pattern comparison.

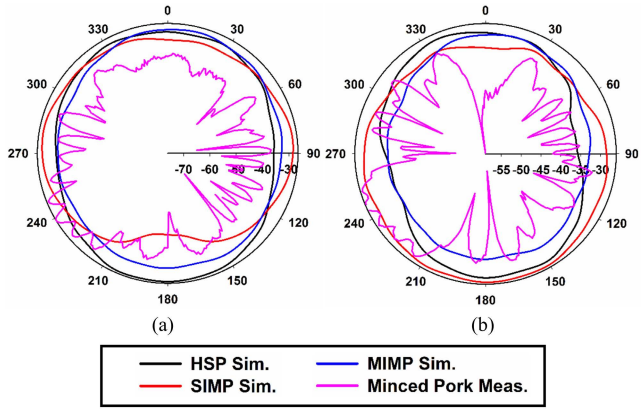

FIGURE 10. Radiation pattern comparison of proposed antenna in different scenarios at 2,450 MHz. (a) YZ (E)-plane, (b) XY (H)-plane.

However, the intended band is still covered, and no modifications are required in the antenna structure, likely because of the full ground plane without any slots resulting in reduced backward radiation. Furthermore, the proposed antenna is resonating at the 2,450 MHz band for the different simulation scenarios. The measured impedance bandwidth covered by the proposed antenna is 262 MHz (2,249–2,511 MHz). Small shifts in the resonance frequency are apparent in Figure 8. They may be mainly due to 1) imperfections in fabrication, 2) air gap that exists between the superstrate and the antenna, 3) electrical properties differences between the minced pork and simulation environment, and 4) cable losses.

In the MIMP, the impedance matching deteriorated more than in the other cases. However, it still covers the band of interest, likely due to the asymmetric loading of the body tissue [3] and the different electrical properties of body layers. Moreover, the measured return loss shifted to 2,400 MHz, likely due to a soldering bump over the patch and the existing air gap between the patch and superstrate, in addition to the fabrication intolerance and measurement inaccuracies [21], [29].

Furthermore, the effects of coaxial cable on the performance of the proposed antenna in the skin phantom (HSP) were investigated because the coaxial cable can affect the impedance matching and radiation performance of electrically-small antennas. The diameters of the inner and outer conductors of the coaxial cable are 0.28 mm and 1.19 mm, respectively. Teflon ($\varepsilon_r = 2.1$ and $\tan\delta = 0.001$) was used as an insulating material between these conductors with a diameter of 0.94 mm. Three cases were considered in simulation, as depicted in Figure 9(a): Case a (antenna without coaxial cable), Case b (antenna with short coaxial cable), and Case c (antenna with long coaxial cable). The simulated return loss and plots of radiation pattern presented in elevation plane are depicted in Figures 9b and 9c, respectively. A slight shift in the resonance frequency and a minute change in the radiation pattern are evident. These changes can be attributed to the coupling between the outer coaxial cable conductor and the biological tissues [30].

Simulated polar plots of the radiation patterns at the operating frequency in the HSP, SIMP and MIMP with the measured once (in minced pork) in the E-plane (YZ) and H (XY) plane are illustrated in Figure 10. The radiation patterns were measured in the anechoic chamber where a high gain horn antenna was the transmitting antenna and the proposed antenna placed inside minced pork meat was the receiving antenna. The radiation patterns in both planes are nearly omnidirectional in HSP, SIMP, and MIMP. In the minced pork meat, however, due to the asymmetric dielectric and conductivity distribution, the omni-directionality of the pattern is disturbed. Omni-directional patterns have the advantage that they can transmit or receive information from any direction. Such kind of radiation pattern is highly desirable in implantable antenna applications. The maximum gain of -26 dBi of the proposed antenna was realized in the skin phantom at the operating frequency. The measured peak gain of the proposed antenna at 2,450 MHz was -26.54 dBi. However, the discrepancy found in the measured radiation patterns in both planes that may be attributed to fabrication intolerance and measurement inaccuracies. In addition it might be due to the asymmetric distribution of permitivity and conductivity of the minced pork meat.

The current distribution of the proposed implantable antenna at the operating frequency is depicted in Figure 11. At the resonance frequency of 2,450 MHz, the whole radiating patch is activated. The figure shows that the current on the patch is flowing in the same direction following the longest path thus insuring a good impedance match and larger electrical length at the resonance frequency. At this frequency, the current does not change its direction, which corresponds to a quarter wavelength monopole mode [3]. The current on the ground plane remains almost uniform at the center with a lower current density. However, a stronger current is focused at the edge of the ground plane close to the feeding point.

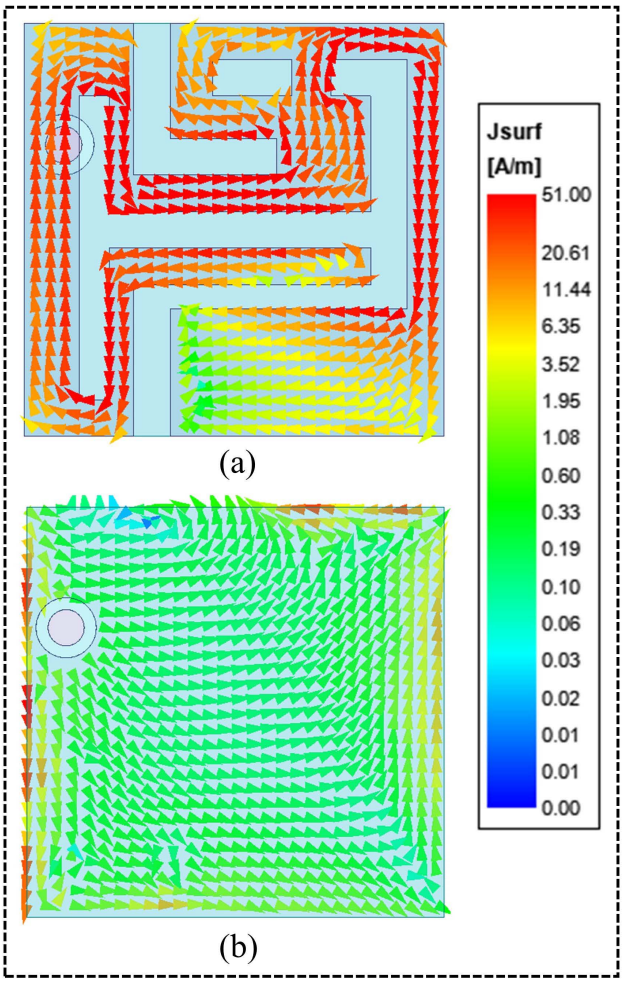

FIGURE 11. Current distribution of the proposed implantable antenna at 2,450 MHz on (a) radiating patch and (b) ground plane.

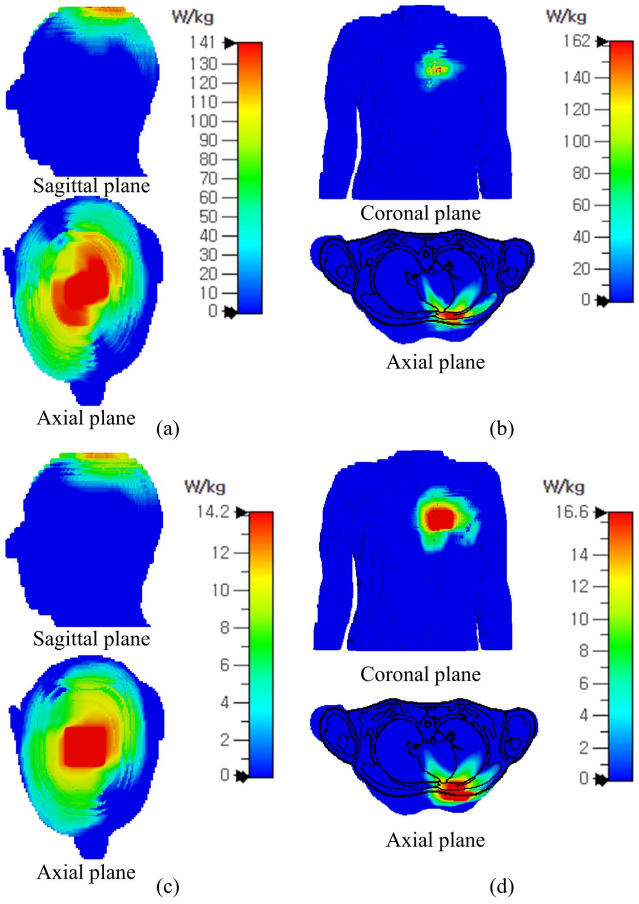

FIGURE 12. Simulated averaged SAR Average over 1 g of tissue (a)–(b) and 10 g of tissue (c)–(d) at 2.45 GHz.

TABLE 3. Maximum peak SAR and maximum allowable input power (input power = 1W).

Implanting tissue	Peak 1-g SAR (W/kg)	Peak 10-g SAR (W/kg)	1-g Maximum allowable power (mW)	10-g Maximum allowable power (mW)
Head	141	14.2	11.34	140.8
Chest	162	16.6	9.87	120.5

Due to the weak current densities on the ground plane, the coupling between the back radiations and the components of the IMD will be very less, therefore, minimal detuning of the operating frequency was observed (as shown in Figure 6).

The use of an implantable antenna can cause electromagnetic energy to accumulate in body tissue. Consequently, it is essential for evaluating patient safety. SAR is regarded as the evaluating standard for implantable antennas. IEEE C-95–1999 and IEEE C-95–2005 confined the SAR values averaged over 1-g and 10-g of human tissue to be less than 1.6 and 2 W/kg, respectively [31]. The SAR distribution at the operating frequency of the proposed antenna was calculated by implanting the antenna in the heterogeneous head with an implantation depth of 5 mm and chest with an implantation depth of more than 10 mm of the Gostove human model in a finite-difference time-domain (FDTD)-based simulator, as depicted in Figure 12.

For the 1-g SAR standard at a 1-W input power in the ISM band of 2,450 MHz, the calculated SAR values were 141 and 162 W/Kg in the head and chest of the Gostove human model, respectively. In contrast, the 10-g SAR values at the operating frequency band were 14.2 and 16.6 W/kg in the head and chest of the Gostove human model, respectively. Table 3 presents the detailed SAR values of the proposed antenna, including the allowed maximum power. These values are much less than existing implantable antennas [10], [16], [18], [19], [20], [21], [22], [23].

For reliable communication with an external base station, analysis of the link budget at three different bit rates (Br): 7 kbps, 100 kpbs, and I Mbps was performed. Input power of 25 μW (−46 dBW) at 2,450 MHz of the implant system was used, and the external antenna had a gain (Gr) of 2.15 dBi. The other values are listed in Table 2. The communication link margin changes against distance are depicted

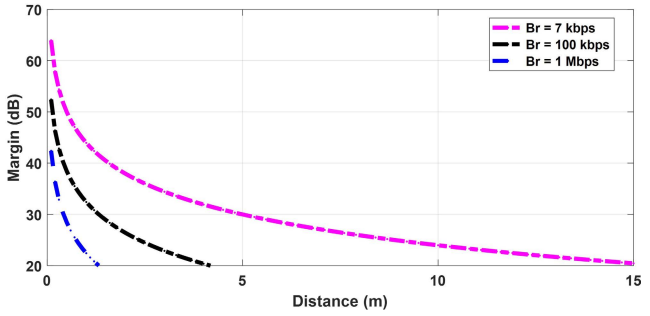

FIGURE 13. Link margin plotted against distance at 2,450 MHz.

in Figure 13. With a 20-dB margin and at bit rates of 7 and 100 kbps, the proposed antenna can communicate at distances of 15 and 4 m, respectively. However, the communication range decreases to 1.3 m when the bit rate increases to 1 Mbps. Based on these results, the proposed implantable antenna system is suitable for the proposed biotelemetry applications.

The dielectric properties of the surrounding human tissues have a major impact on the performance of an implantable antenna. Therefore, accurate antenna performance analysis must be conducted under different tissue loading conditions. Hence, the permittivity (ε_r) and conductivity (σ) of the HSP varied from 50% to 150% as shown in Figures. 14(a) and 14(b), respectively. Figure 14(a) clearly shows that as ε_r increases and decreases the resonance shifts towards the lower and upper frequencies, respectively. This is the result of the inverse relationship between ε_r and resonance frequency as given in Eq. (1).

$$f_r = \frac{c}{L_g\sqrt{\frac{\varepsilon_r+1}{2}}} \tag{4}$$

where *fr, c, Lg,* and ε_r represent resonance frequency, speed of EM wave in free space, length of the antenna, and combined relative permittivity of the dielectric and superstrate, respectively. Similarly, to analyze the effect of σ on the performance of the antenna, it was varied from 50% to 150% as depicted in Figure 14 (b). As clear from the figure variation of σ has a minimum effect on the resonance frequency of the proposed antenna. The variation only affects the impedance matching [20] resulting in an increase or decrease in the depth of reflection coefficient (S11). Additionally, the tanδ of the tissue is also affected by both ε_r and σ as given by Eq. (2).

$$tan\delta = \frac{\sigma}{\varepsilon_r\varepsilon_0\omega} \tag{5}$$

where ε_0 and ω are the free-space permittivity and frequency in radian, respectively. The results presented in Figure 14 show that the proposed antenna can offer stable performance when the antenna is placed in locations having different varying tissue conditions.

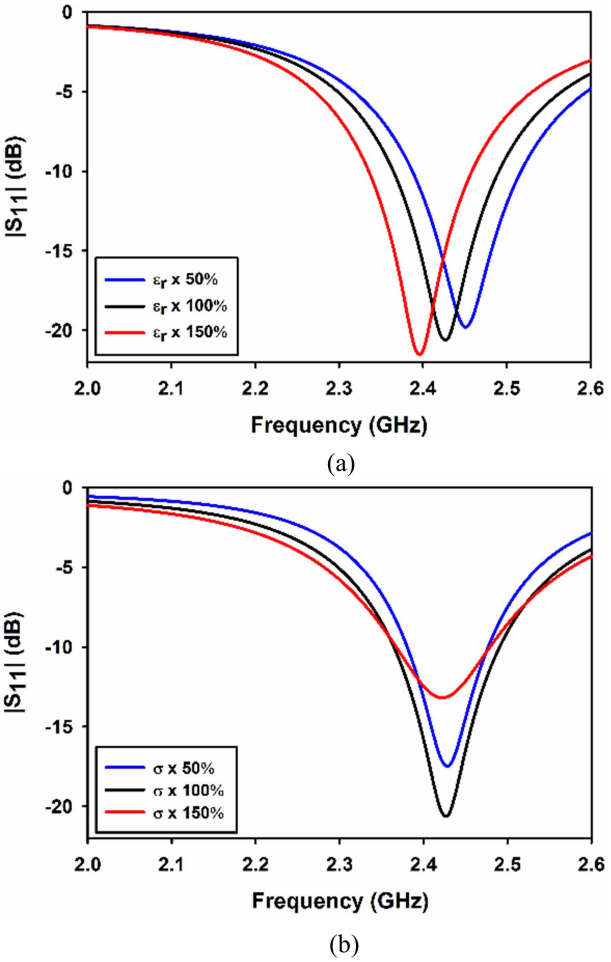

FIGURE 14. Sensitivity evaluation of the proposed antenna by varying (a) permittivity and (b) conductivity of the tissue.

IV. CONCLUSION

This paper presented an ultra-miniaturized implantable antenna for biotelemetry applications at the 2,450 MHz band. A high permittivity substrate/superstrate and meandered patch resulted in a compact size of 3.45 × 3.4 × 0.377 mm (4.422 mm^3). The antenna's performance with and without integration with dummy electronics and batteries was analyzed in three types of phantoms: HSP, SIMP, and MIMP.

Moreover, coaxial cable effects on the proposed antenna performance were studied. The antenna was fabricated, and measurements were taken in saline solution and minced pork for return loss, radiation pattern, and SAR, which agreed closely with the simulated results. Based on the results obtained and its compact size, the proposed antenna could be an excellent candidate for intended biotelemetry applications.

ACKNOWLEDGMENT

(Syed Manaf Ali Shah and Muhammad Zada are co-first authors.)

REFERENCES

[1] A. Kiourti, K. A. Psathas, and K. S. Nikita, "Implantable and ingestible medical devices with wireless telemetry functionalities: A review of current status and challenges," *Bioelectromagnetics*, vol. 35, no. 1, pp. 1–15, Jan. 2015.
[2] F. Faisal, M. Zada, A. Ejaz, Y. Amin, S. Ullah, and H. Yoo, "A miniaturized dual-band implantable antenna system for medical applications," *IEEE Trans. Antennas Propag.*, vol. 68, no. 2, pp. 1161–1165, Feb. 2020.
[3] I. A. Shah, M. Zada, and H. Yoo, "Design and analysis of a compact-sized multiband spiral-shaped implantable antenna for scalp implantable and leadless pacemaker systems," *IEEE Trans. Antennas Propag.*, vol. 67, no. 6, pp. 4230–4234, Jun. 2019.
[4] H. Bahrami, S. A. Mirbozorgi, R. Ameli, L. A. Rusch, and B. Gosselin, "Flexible, polarization-diverse UWB antennas for implantable neural recording systems," *IEEE Trans. Biomed. Circuits Syst.*, vol. 10, no. 1, pp. 38–48, Feb. 2016.
[5] B. Chi, J. Yao, S. Han, X. Xie, G. Li, and Z. Wang, "Low-power transceiver analog front-end circuits for bidirectional high data rate wireless telemetry in medical endoscopy applications," *IEEE Trans. Biomed. Eng.*, vol. 54, no. 7, pp. 1291–1299, Jul. 2007.
[6] ITU. (2022). *Technical and Operating Parameters and Spectrum Use for Short-Range Radiocommunication Devices*. Accessed: Mar. 4, 2022. [Online]. Available: https://www.itu.int/pub/R-REP-SM.2153-8-2021
[7] D. Nguyen and C. Seo, "An ultra-miniaturized antenna using loading circuit method for medical implant applications," *IEEE Access*, vol. 9, pp. 111890–111898, 2021.
[8] S. Hout and J.-Y. Chung, "Design and characterization of a miniaturized implantable antenna in a seven-layer brain phantom," *IEEE Access*, vol. 7, pp. 162062–162069, 2019.
[9] S. Das and D. Mitra, "A compact wideband flexible implantable slot antenna design with enhanced Gain," *IEEE Trans. Antennas Propag.*, vol. 66, no. 8, pp. 4309–4314, Aug. 2018.
[10] V. Kaim, B. K. Kanaujia, S. Kumar, H. C. Choi, K. W. Kim, and K. Rambabu, "Ultra-miniature circularly polarized CPW-fed implantable antenna design and its validation for biotelemetry applications," *Sci. Rep.*, vol. 10, no. 1, pp. 1–16, Dec. 2020.
[11] Y. Fan, J. Huang, T. Chang, and X. Liu, "A miniaturized four-element MIMO antenna with EBG for implantable medical devices," *IEEE J. Electromagn., RF, Microw. Med. Biol.*, vol. 2, no. 4, pp. 226–233, Dec. 2018.
[12] A. J. Alazemi and A. Iqbal, "A high data rate implantable MIMO antenna for deep implanted biomedical devices," *IEEE Trans. Antennas Propag.*, vol. 70, no. 2, pp. 998–1007, Feb. 2022.
[13] L. Amjad, M. A. Hasan, I. B. Mabrouk, and M. Nedil, "Scalp-implantable MIMO antenna for high-data-rate head implants," *IEEE Antennas Wireless Propag. Lett.*, vol. 20, no. 12, pp. 2529–2533, Dec. 2021.
[14] M. Al-Hasan, P. R. Sura, A. Iqbal, J. J. Tiang, I. B. Mabrouk, and M. Nedil, "Low-profile dual-band implantable antenna for compact implantable biomedical devices," *AEU-Int. J. Electron. Commun.*, vol. 138, Aug. 2021, Art. no. 153896.
[15] M. Yousaf, I. B. Mabrouk, F. Faisal, M. Zada, Z. Bashir, A. Akram, M. Nedil, and H. Yoo, "Compacted conformal implantable antenna with multitasking capabilities for ingestible capsule endoscope," *IEEE Access*, vol. 8, pp. 157617–157627, 2020.
[16] N. Abbas, S. A. A. Shah, A. Basir, Z. Bashir, A. Akram, and H. Yoo, "Miniaturized antenna for high data rate implantable brain-machine interfaces," *IEEE Access*, vol. 10, pp. 66018–66027, 2022, doi: 10.1109/ACCESS.2022.3184778.
[17] S. M. A. Shah, M. Zada, J. Nasir, and H. Yoo, "Ultra-miniaturized triband antenna with reduced SAR for skin and deep tissue implants," *IEEE Trans. Antennas Propag.*, early access, May 30, 2022, doi: 10.1109/TAP.2022.3177487.
[18] N. Abbas, A. Basir, A. Iqbal, M. Yousaf, A. Akram, and H. Yoo, "Ultra-miniaturized antenna for deeply implanted biomedical devices," *IEEE Access*, vol. 10, pp. 54563–54571, 2022, doi: 10.1109/ACCESS.2022.3176720.
[19] L.-J. Xu, Y. Bo, W.-J. Lu, L. Zhu, and C.-F. Guo, "Circularly polarized annular ring antenna with wide axial-ratio bandwidth for biomedical applications," *IEEE Access*, vol. 7, pp. 59999–60009, 2019.
[20] M. Yousaf, I. B. Mabrouk, M. Zada, A. Akram, Y. Amin, M. Nedil, and H. Yoo, "An ultra-miniaturized antenna with ultra-wide bandwidth characteristics for medical implant systems," *IEEE Access*, vol. 9, pp. 40086–40097, 2021, doi: 10.1109/ACCESS.2021.3064307.
[21] M. Zada, I. A. Shah, A. Basir, and H. Yoo, "Ultra-compact implantable antenna with enhanced performance for leadless cardiac pacemaker system," *IEEE Trans. Antennas Propag.*, vol. 69, no. 2, pp. 1152–1157, Feb. 2020.
[22] R. Liu, K. Zhang, Z. Li, W. Cui, W. Liang, M. Wang, C. Fan, H. Zheng, and E. Li, "A wideband circular polarization implantable antenna for health monitor microsystem," *IEEE Antennas Wireless Propag. Lett.*, vol. 20, no. 5, pp. 848–852, May 2021.
[23] Z. Xia, H. Li, Z. Lee, S. Xiao, W. Shao, X. Ding, and X. Yang, "A wideband circularly polarized implantable patch antenna for ISM band biomedical applications," *IEEE Trans. Antennas Propag.*, vol. 68, no. 3, pp. 2399–2404, Mar. 2020.
[24] M. Zada, I. A. Shah, and H. Yoo, "Metamaterial-loaded compact high-gain dual-band circularly polarized implantable antenna system for multiple biomedical applications," *IEEE Trans. Antennas Propag.*, vol. 68, no. 2, pp. 1140–1144, Feb. 2020.
[25] C. Gabriel, S. Gabriel, and E. Corthout, "The dielectric properties of biological tissues: I. Literature survey," *Phys. Med. Biol.*, vol. 41, no. 11, p. 2231, 1996.
[26] R. Das and H. Yoo, "A wideband circularly polarized conformal endoscopic antenna system for high-speed data transfer," *IEEE Trans. Antennas Propag.*, vol. 65, no. 6, pp. 2816–2826, Jun. 2017.
[27] M. Zada and H. Yoo, "Miniaturized dual band antennas for intra-oral tongue drive system in the ISM bands 433 MHz and 915 MHz: Design, safety, and link budget considerations," *IEEE Trans. Antennas Propag.*, vol. 67, no. 9, pp. 5843–5852, Sep. 2019.
[28] M. Zada, I. A. Shah, A. Basir, and H. Yoo, "Simultaneous wireless power transfer and data telemetry using dual-band smart contact lens," *IEEE Trans. Antennas Propag.*, vol. 70, no. 4, pp. 2990–3001, Apr. 2022.
[29] A. Basir, M. Zada, Y. Cho, and H. Yoo, "A dual-circular-polarized endoscopic antenna with wideband characteristics and wireless biotelemetric link characterization," *IEEE Trans. Antennas Propag.*, vol. 68, no. 10, pp. 6953–6963, Oct. 2020.
[30] C. Liu, Y.-X. Guo, and S. Xiao, "Capacitively loaded circularly polarized implantable patch antenna for ISM band biomedical applications," *IEEE Trans. Antennas Propag.*, vol. 62, no. 5, pp. 2407–2417, May 2014.
[31] K. Liu, R. Liu, W. Cui, K. Zhang, M. Wang, C. Fan, H. Zheng, and E. Li, "Design of conformal spiral dual-band antenna for wireless capsule system," *IEEE Access*, vol. 9, pp. 117349–117357, 2021.

SYED MANAF ALI SHAH received the B.Sc. degree in telecommunication from Hazara University, Dhodial, Mansehra, Pakistan, in 2016, and the M.S. degree in electrical engineering from the Department of Electrical Engineering, COMSATS University, Islamabad, Abbottabad, Pakistan, in 2021. His research interests include printed antennas, flexible antennas, implantable antennas, MIMO antennas, dielectric resonator antennas, wireless power transfer, and synthesis of microwave components.

MUHAMMAD ZADA (Graduate Student Member, IEEE) received the B.Sc. degree in telecommunication engineering from the University of Engineering and Technology, Peshawar, Pakistan, in 2015. He is currently pursuing the M.S./Ph.D. degree in electronic engineering with Hanyang University, Seoul, South Korea.

He has published over 20 papers in high-quality journals and conference proceedings in the field of telecommunications, electronic, and biomedical engineering. He is serving as a reviewer for IEEE Transactions, RFCAD, and Elsevier journals. His current research interests include implantable antennas and devices, intra-oral tongue drive systems, wireless power transfer, millimeter-wave antennas, wearable sensors and antennas, smart contact lenses, smart-textile, MRI and RF coils, microwave breast cancer detection, frequency-selective surfaces, and EBGs. He was awarded the Best Student Paper Competition 2018 from the Korean Institute of Electromagnetic Engineering and Science (KIEES).

JAMAL NASIR was born in Malakand, Khyber Pakhtunkhwa, Pakistan, in 1983. He received the M.Sc. degree in mobile and satellite communication from the University of Bradford, U.K., in 2007, and the Ph.D. degree in electrical engineering from Universiti Teknologi Malaysia, in 2017. He is currently an Assistant Professor with the Department of Electrical Engineering, COMSATS University Islamabad, Abbottabad Campus, Khyber Pakhtunkhwa. His research interests include SIW-based passive components and arrays, metamaterials, smart antennas, mutual coupling analysis, MIMO antennas, dielectric resonator antennas, UWB antennas, slotted waveguide arrays, ingestible and Implantable antennas, and wearable antennas.

OWAIS OWAIS received the B.E. and master's degrees from the University of Engineering and Technology, Peshawar, Pakistan, in 1996 and 2000, respectively, and the Ph.D. degree in communication electronics from the Department of Science and Technology, Linköping University, Sweden. He is currently serving as an Associate Professor with the COMSATS University Islamabad, Abbottabad Campus, Pakistan. He has authored 40 international journal articles. His main research interests include the design of microstrip patch and dielectric resonator antennas, MIMO and reconfigurable DRAs, electromagnetic bandgap, and double-negative metamaterials; moreover, six-port front-end circuits for direct conversion transceiver design and high-speed data transmissions are also his area of interest.

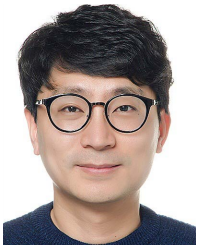

HYOUNGSUK YOO (Senior Member, IEEE) received the B.Sc. degree in electrical engineering from Kyungpook National University, Daegu, South Korea, in 2003, and the M.Sc. and Ph.D. degrees in electrical engineering from the University of Minnesota, Minneapolis, MN, USA, in 2006 and 2009, respectively.

In 2009, he joined the Center for Magnetic Resonance Research, University of Minnesota, as a Postdoctoral Associate. In 2010, he joined Cardiac Rhythm Disease Management, Medtronic, MN, USA, as a Senior EM/MRI Scientist. From 2011 to 2018, he was an Associate Professor at the Department of Biomedical Engineering, School of Electrical Engineering, University of Ulsan, Ulsan, South Korea. Since 2018, he has been a Full Professor with the Department of Biomedical Engineering and the Department of Electronic Engineering, Hanyang University, Seoul, South Korea. He has been the CEO of E2MR, a startup company, since 2017. His current research interests include electromagnetic theory, numerical methods in electromagnetics, metamaterials, antennas, implantable devices, and magnetic resonance imaging in high-magnetic field systems.

Dr. Yoo was awarded Third Prize for the Best Student Paper at the 2010 IEEE Microwave Theory and Techniques Society and International Microwave Symposium.